Journal of Biomechanics 171 (2024) 112181

Contents lists available at ScienceDirect

Journal of Biomechanics

journal homepage: www.elsevier.com/locate/jbiomech

Advanced subject-specific neck musculoskeletal modeling unveils sex differences in muscle moment arm and cervical spine loading

Curran Reddy [a], Yu Zhou [b], Wei Yin [b], Xudong Zhang [a,b,c,*]

[a] Department of Biomedical Engineering, Texas A&M University, USA
[b] Department of Industrial and Systems Engineering, Texas A&M University, USA
[c] Department of Mechanical Engineering, Texas A&M University, USA

ARTICLE INFO

Keywords:
Neck strength
Musculoskeletal modeling
Sex differences
Subject-specificity
Muscle moment arm
Spinal compression

ABSTRACT

Neck pain and injuries are growing healthcare burdens with women having a higher incidence rate and poorer treatment outcomes than males. A better understanding of sex differences in neck biomechanics, foundational for more targeted, effective prevention or treatment strategies, calls for more advanced subject-specific musculoskeletal modeling. Current neck musculoskeletal models are based on generic anatomy, lack subject specificity beyond anthropometric scaling, and are unable to accurately reproduce neck strengths exhibited *in vivo* without arbitrary muscle force scaling factors or residual torque actuators. In this work, subject-specific neck musculoskeletal models of 23 individuals (11 male, 12 female) were constructed by integrating multi-modality imaging and biomechanical measurements. Each model simulated maximal voluntary neck static exertions in three postures: neck flexion in a neutral posture, flexion in a 40° extended posture, and extension in a 40° flexed posture. Quantitative model validation showed close agreement between model-predicted muscle activation and EMG measurement. The models unveiled that (1) males have greater moment arms in one flexor muscle group and five extensor muscle groups, (2) females exhibited higher cervical spinal compression per unit exertion force in the flexed posture, and (3) the variability of compression force was much greater in females in all three exertions but most notably in the extension with a flexed "dropped head" position. These insights illuminated a plausible pathway from sex differences in neck biomechanics to sex disparities in the risk and prevalence of neck pain.

1. Introduction

Neck pain and injury are growing healthcare burdens and affecting females more than males (Côté et al., 2004; Dieleman et al., 2016; Hoy et al., 2014; Hurwitz et al., 2018; Murray et al., 2013; Vos et al., 2012). The global prevalence of neck pain is estimated to be 4.8 %, 3.9 % in males and 5.7 % in females; in North America, the incidence rates are even higher and exhibiting a more alarming sex disparity: 5.3 % and 7.6 % in males and females, respectively (Hoy et al., 2014; Vos et al., 2012). In addition to being more likely to suffer from neck pain, females are at greater risk of neck injury from impact and are more likely to have persistent neck pain (Berglund et al., 2006; Dolinis, 1997; Hendriks et al., 2005). The treatment of non-specific, mechanical neck pain cannot yet be characterized as successful, and females have significantly poorer outcomes than males (Barreto and Svec, 2019; Evans, 2014; Hendriks et al., 2005; Ylinen et al., 2003). Neck muscular strength is believed to be an important modifiable factor in injury prevention strategies and pain treatment protocols, and likely to play a role in the observed epidemiological sex differences (Côté, 2012). Personalization, by way of targeting specific preventative or therapeutic strengthening interventions according to an individual's unique neck anatomy and physiology, may hold the key to discovering successful protocols. An improved basic understanding of sex differences in neck biomechanics, particularly with respect to muscular strength, can shed new light on the efficacy of personalized interventions and sex disparities in neck pain prevalence and treatment outcomes. Such an understanding calls for subject-specific musculoskeletal modeling.

Musculoskeletal modeling software tools like OpenSim and AnyBody have become the standard platforms for testing hypotheses, addressing what-if questions, and streamlining inverse dynamics calculations and subsequent muscle activation approximation (Seth et al., 2011). The latest neck biomechanical model built in OpenSim, the HYOID model,

* Corresponding author at: 4077 Emerging Technologies Building, 3131 TAMU, College Station, TX 77843-3131, USA.
E-mail addresses: creddy12@tamu.edu (C. Reddy), yuznick96@tamu.edu (Y. Zhou), yinwei@tamu.edu (W. Yin), xudongzhang@tamu.edu (X. Zhang).

https://doi.org/10.1016/j.jbiomech.2024.112181
Accepted 4 June 2024
Available online 6 June 2024

remains limited in its level of subject-specificity. It is built using generic anatomical data and muscle force generating properties and only facilitates scaling based on anthropometry (Kamibayashi and Richmond, 1998; Mortensen et al., 2018). As an example, the morphology of the clavicle of the HYOID model is generic, as are the landmarks that define muscle-bone attachment sites; thus, the one-dimensional representations of muscle paths are not specific to a given subject but simply scaled to best fit the individual's anthropometry. As for the maximum force production capacity, all OpenSim models use a single constant for maximum muscle stress across all muscles and all individuals (Seth et al., 2018; Seth et al., 2011; Zajac, 1989). Existing neck models that employ a forward dynamics approach for strength estimation require reserve actuators or scaling factors to replicate force values measured from human strength testing; the HYOID model must multiply extensor strength by a factor of 1.4 and flexor strength by a factor of 2.7 to match experimentally obtained force outputs (Mortensen et al., 2018).

While scaling factors may not inherently invalidate a model, the application of generic muscle force generating parameters undermines the investigation of individual variation in the biomechanical basis of neck strength. Some progress toward improved specificity has been made by way of creating a female-specific neck model (Zheng et al., 2013). However, the model was constructed using generic female anatomy without accounting for individual anatomical variability beyond anthropometry. Attempts to personalize force generating properties, by scaling physiological cross-sectional area (PCSA) values with subject-specific muscle volumes, have been marginally effective in shoulder modeling and achieved little success in neck modeling (Bolsterlee et al., 2015; Netto et al., 2008). The lack or insufficiency of subject-specificity in current neck models precludes investigation of sex or individual differences in neck structure, function, and biomechanics. The development of more advanced subject-specific models, with minimal generic or arbitrary values quantifying anatomy, musculoskeletal geometry, and force generating capacity, is needed for identifying and understanding the differences and exploring more effective, targeted intervention or prevention strategies (e.g., sex-specific or personalized muscle strengthening therapies and wearables to promote or prevent certain positions or movements).

Therefore, in this study, we aimed to develop highly subject-specific neck biomechanical models, for a cohort of subjects in static maximum voluntary flexion–extension exertions, by harnessing musculoskeletal imaging and modeling tools. With these models and a gender-balanced experimental design, we also sought to elucidate the sex differences in neck muscle geometry and biomechanics and their potential effects on risk for injury.

2. Methods

2.1. Data acquisition

The data used for developing the neck biomechanical models and in the subsequent model-based analysis were acquired from an experiment (Chowdhury et al., 2021; Reddy et al., 2021; Zhou et al., 2020a) in which participants underwent two medical imaging sessions and a biomechanical testing session. High resolution computed tomography (CT) and magnetic resonance imaging (MRI) scans of participants' neck regions were obtained to provide detailed bone and soft tissue morphological information, respectively. In the biomechanical testing session, participants performed static maximum voluntary contractions (MVCs) in the following neck exertion direction and posture conditions: flexion in a neutral posture (Neu), flexion in 40° of head-neck extension (Ext), and extension in 40° of flexion (Flex). These exertions were performed against a multi-axial load cell via a custom-made helmet worn by participants while they were seated with their torsos restrained. The helmets had four different sizes to accommodate varied head anthropometry and were mounted with 3D-printed plastic spherical protrusions at the front and back that allowed for accurate, consistent positioning and mating with a spherical cavity attached to the load cell. Details and rationale for this design were described in Zhou et al., (2020a). In addition to the static exertions, participants performed free full-range flexion–extension movements. While these exertions and motions were performed, a dynamic stereo radiography (DSX) system, motion capture (MoCap) system, and surface electromyography (EMG) system simultaneously measured cervical vertebral kinematics, surface-marker-based kinematics, and neck muscle activity, respectively. For MoCap measurement, three surface markers were placed on the helmet (front, top, right), five on the head (forehead, left and right infraorbitals, left and right tragion notches), and four on the rest of the body (C7, sternum, left and right shoulders). A total of eight EMG electrodes were placed on the skin overlying the infrahyoids (Hyoid), sternocleidomastoid (SCM), splenius capitis (SPL), and upper trapezius (Trap) muscles bilaterally.

From the original database consisting of 40 healthy adults (Chowdhury et al., 2021), twenty-three (11 males and 12 females, aged 21 – 45) were selected for this study based on criteria that included adequate MRI quality for muscle border distinction, sufficient DSX image quality for tracking all 7 vertebrae, acceptable number of MoCap markers for tracking head and load cell positions, and proper task execution verified by force measurement. The study protocol, approved by the Institutional Review Board, was explained in detail to the participants who all provided written consent.

2.2. Model development

The development of subject-specific models integrated CT, MRI, DSX, motion capture, load cell, and EMG data and proceeded in four distinct steps: (1) CT-MRI co-registration, (2) posture-dependent muscle geometry specification, (3) optimization-based muscle redundancy solution, and (4) EMG-based model validation.

2.2.1. CT-MRI co-registration

Three-dimensional (3D) point cloud representations of involved neck muscles, reconstructed from MRI (Reddy et al., 2021), were co-registered with 3D bone models of cervical vertebrae reconstructed from CT. This was required to define muscle paths in relation to vertebral position and orientation or, grossly, one's neck posture, and could not be done with MRI alone because the vertebral bone models segmented from MRI suffered from substantial volume loss, missing structural details critical for anchoring muscle paths. The challenge associated with co-registration of a complex, high-degree-of-freedom structure like the cervical spine is that the poses adopted during the two imaging modalities are never identical (Zhou et al., 2019). A pose-matching co-registration procedure (Zhou et al., 2020b) was implemented for each participant. The procedure searched through a series of frames of CT-based bone models of varying poses, obtained from the DSX recording of the full-range flexion–extension motion, for the one frame in which the cervical spine curvature best matched that of the MRI-based bone model. The curvature was characterized by first fitting least-squares circles to vertebral foramina from C1 to C7 and then curve-fitting the centroids of all vertebrae with a cubic polynomial. The best match was identified as having the minimum curvature discrepancy, quantified as the Fréchet distance (Eiter and Mannila, 1994) between the two 3D polynomials.

2.2.2. Posture-dependent muscle geometry specification

After co-registration, individual muscle paths were defined in reference to vertebral positions and orientations. MRI-based muscle path identification utilized a segmentation and reconstruction-based technique (Reddy et al., 2021) to generate a cubic polynomial curve for each muscle (Fig. 1). Doing so for all muscles for a given vertebra created a cross-sectional "snapshot" of muscle positions at the vertebral level. Thus, DSX-measured vertebral positions and orientations served as bases for predicting muscle path geometry. This strategy is an adaptation of

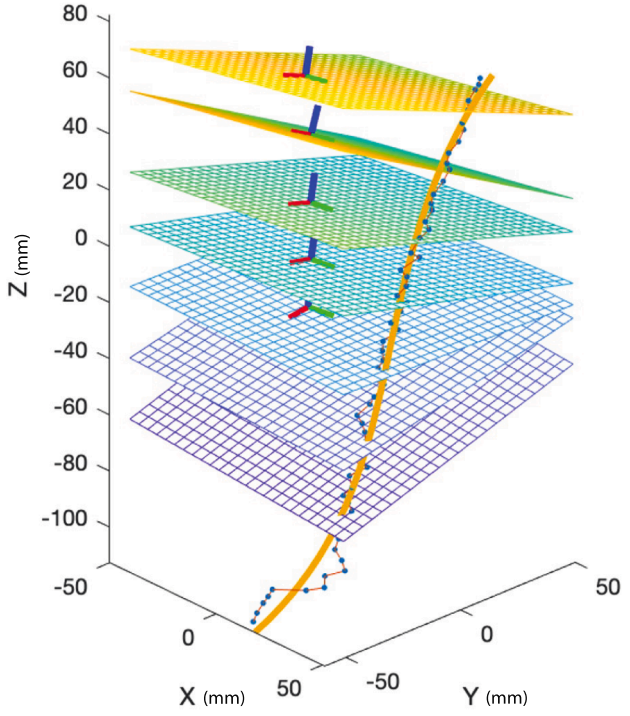

Fig. 1. Local coordinate systems (LCSs) were established for each CT-segmented vertebra by a principal component analysis of the point clouds (with X positive anteriorly, Y positive left laterally, and Z positive superiorly—units in mm). A 3D polynomial was then fit to the centroids of slices (slice thickness: 3 mm) of each MRI-based muscle model (blue dots connected by red lines). The intersection this polynomial (gold curve) and a vertebra's "transverse" (XY) plane was designated as the "via-point" for the muscle in the corresponding vertebral LCS; thus, muscles spanning the entire length of the cervical spine had seven via-points. The left sternocleidomastoid is shown here as an example. (For interpretation of the references to colour in this figure legend, the reader is referred to the web version of this article.)

the moving muscle points (MMP) approach using vertebral kinematics in lieu of MRI imaging of the neck in multiple postures (Suderman and Vasavada, 2017). This quasi-via-points muscle representation is also a departure from the one-dimensional approach in OpenSim and allows for more precise moment arm calculation (Suderman et al., 2012).

Upon defining via-points in vertebral LCSs, DSX-derived vertebral kinematics were used to reconstruct muscle paths, defined using polynomial curves, in various exertion postures (Fig. 2). Among multiple methods available for muscle moment arm calculation (Ackland et al., 2011; Ingram et al., 2015), the geometric method (wherein moment arm is measured as the perpendicular distance from the muscle line of action and the joint) was chosen for its simplicity and the fact that it allows for moment arm calculation about a spinal joint of choice. In the present study, moments were resolved about the centroid of the C6 vertebra; however, the models were constructed in a manner that permits alternative choices of vertebral level as the reference origin.

2.2.3. Muscle force and cervical spine disc force determination

The external forces applied to the models included gravitational force due to head mass and exertion reactive force. The head mass was estimated using skull circumference and literature data (Connor et al., 2020; Yoganandan et al., 2009). The center of mass of the head was defined as the midpoint of the left and right tragion notches (where LTra and RTra markers were placed) (Yoganandan et al., 2009). The load cell force vector acted on the head-neck system at the midpoint of the forehead and front of helmet markers for the Neu and Ext positions. For the Flex position, the load cell point of contact was calculated as the forehead marker reflected about the coronal plane. The direction of the force vector in all postures was determined by intersection of the midsagittal plane and the Frankfort plane (as defined by the LTra, RTra, right infraorbital, and left infraorbital markers).

Once the external forces and their lines of action were determined and muscle geometry characterized, a system of equations for static equilibrium was generated, which took the following form:

$$\vec{M}(t) = \vec{r}^{E} \times \vec{F}^{E} + \vec{r}^{H} \times \vec{F}^{H} + \sum_{i=1}^{m} \vec{r}_i^{M} \times \vec{F}_i^{M} + \sum_{i=1}^{s} \vec{r}_i^{S} \times \vec{F}_i^{S} \quad (1)$$

$$\vec{F}(t) = \vec{F}^{E} + \vec{F}^{H} + \sum_{i=1}^{m} \vec{F}_i^{M} + \sum_{i=1}^{s} \vec{F}_i^{S} \quad (2)$$

where equations (1) and (2) respectively describe moment and force equilibria in the coordinate system defined with respect to the C6 vertebra. The terms m and s represent the number of muscles and spinal forces involved. $\vec{F}^{E}$, $\vec{F}^{H}$, $\vec{F}^{M}$, and $\vec{F}^{S}$ represent exertion force, head weight, muscle tensions, and spinal forces, respectively. m is the number of muscles modeled, and s is the number of noncontractile tissue components (e.g., ligaments, cartilage, intervertebral discs) involved in stabilizing the system. $\vec{r}^{E}$, $\vec{r}^{H}$, $\vec{r}^{M}$, and $\vec{r}^{S}$ represent the corresponding moment arms of the aforementioned forces. Note that the spinal forces, compression and shear, generated by the loading of passive tissues were modeled as three "lump sums" or grouped vectors passing through the point at which rotational equilibrium was calculated, C6 in this case; thus, their moment arms are null, and the right-most term of (Eqn. (1) is reduced to 0. Given that the tasks were flexion and extension exertions, only moment about the mediolateral axis was considered in solving for muscle tensions.

Upon defining the system of equations for static equilibrium, the tensions of the individual muscles were solved using an optimization algorithm. While there are different choices for the objective function (Bean et al., 1988; Erdemir et al., 2007), this study utilized the objective function of minimizing the sum of muscle stresses cubed (Eqn. (3) (Hughes et al., 1994; Millard et al., 2013). This objective function has been widely used for muscle force prediction models under volitional conditions, including models built in OpenSim (Seth et al., 2018; Seth et al., 2011). The present study strove to refrain from using generic values for muscle properties in the models and achieve the highest level of subject specificity possible; to this end, a recently proposed new measure, termed reconstruction-based cross-sectional area (RCSA), was used to calculate muscle stress (Reddy et al., 2021).

$$U = \sum_{i=1}^{m} \left(\frac{F_i}{RCSA_i} \right)^3 \quad (3)$$

A lower bound of 0 restricted muscle stress to only tension, and a nominal (not reached) upper bound of 175 N/cm^2 was also placed (Maganaris et al., 2001). Once muscle tensions were resolved to meet the moment equilibrium with respect to the center of C6, cervical intervertebral disc compression and shear forces were estimated by satisfying the force equilibrium, as done in an established low back spinal force estimation approach (McGill and Norman, 1987). This method avoids the "residual activator" or "scaling" problem prior neck musculoskeletal models (e.g., the HYOID neck model in OpenSim) have faced as this method's maximum allowable muscle stress is not constrained to a single value but can vary from individual to individual.

2.2.4. EMG-based model validation

Normalized EMG amplitude was compared to normalized muscle stress (Hughes et al., 1994; Lund et al., 2012; Saraswat et al., 2010). EMG signals were filtered using a 10–500 Hz Butterworth bandpass filter and notch filters 60 Hz intervals to remove noise and power line interference, and amplitudes were quantified as RMS over a 50 ms interval

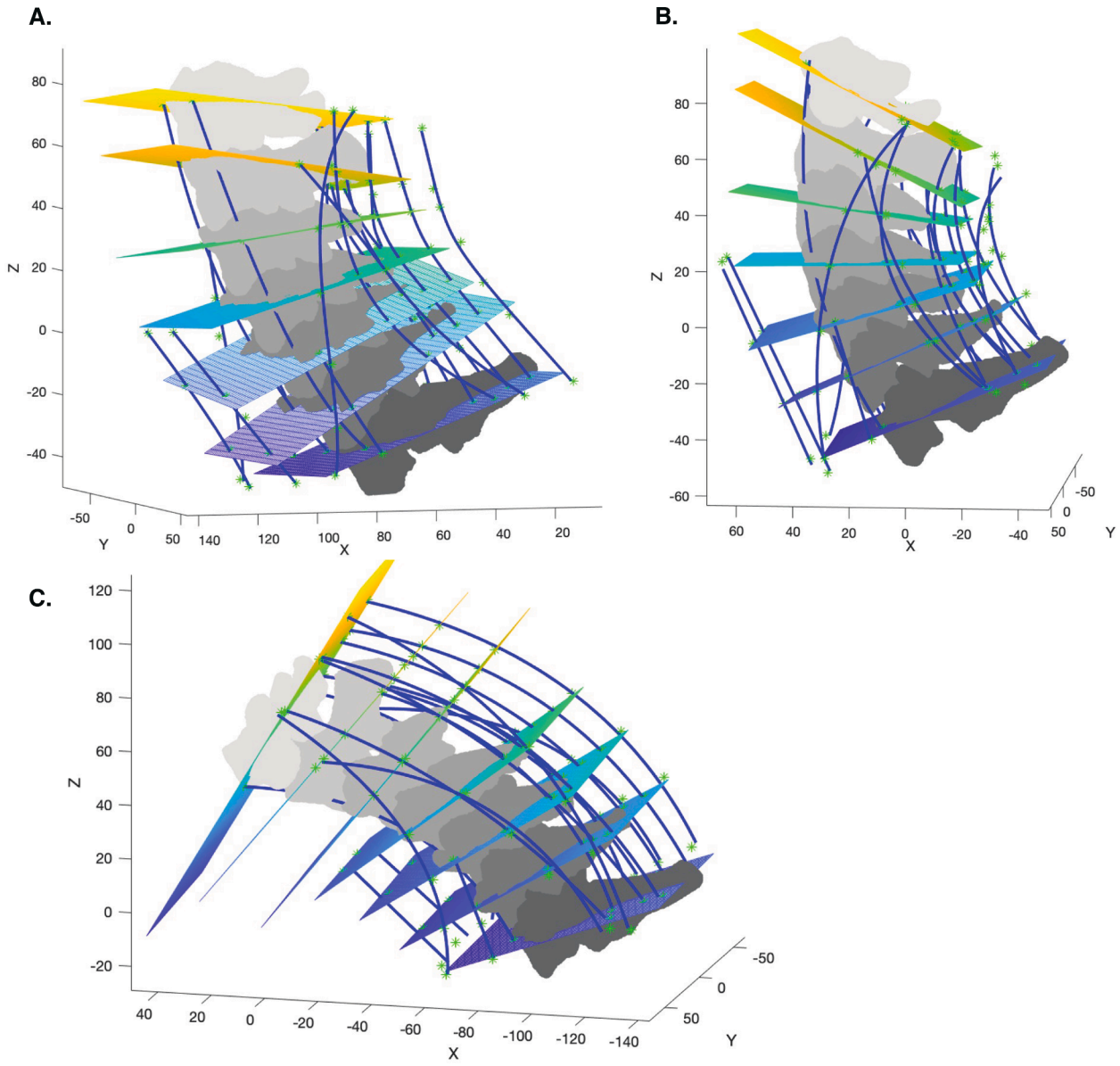

Fig. 2. Reconstructed muscle paths fit to via-points as determined by vertebral kinematics in Neutral (A), Extended (B), and Flexed (C) postures (unit: mm). A polynomial was fit to the via points to redefine the new muscle path in the actual, adopted posture.

(Clancy et al., 2002). EMG amplitude was normalized to muscle-specific maximum recorded amplitude across all trials and then averaged across left and right. Muscle stress was normalized to the highest model-estimated stress for that specific muscle across all trials—termed "specific tension." This yielded a pseudo-% activation metric, better comparable to EMG. Therefore, a subject-specific optimization approach was used to generate normalized muscle stress curves for each muscle in each trial, for a specific subject. Normalized stresses for the SCM, Hyoid, SPL, and Trap muscles were also averaged across left and right sides. Normalized activation and stress profiles for the four muscles were resampled to generate 100 data points for each trial to facilitate comparison across varied exertion durations.

2.3. Model-based analysis and hypothesis testing

Model accuracy was reported as root mean square error (RMSE), calculated for each muscle comparing %-activation (EMG amplitude compared to muscle stress) for each trial. RMSEs were then averaged for each sex for each muscle. A prerequisite for model-based analysis is that model accuracy is consistent across subjects; individual RMSEs were inspected to confirm that no bias was present. Spinal compression forces were calculated as peak compression over a 0.5 s interval and were normalized to exertion force over the same interval. Student's t-tests with an α level of 0.05 were used to identify significant male–female differences in muscle moment arms and spinal compression forces.

3. Results

3.1. Model validation and accuracy

The subject-specific models recreated muscle tension profiles that closely resembled EMG-measured muscle activity (Fig. 3), including the ramp-up, sustained hold, and relaxation phases, for agonist muscles (SCM and Hyoid in flexion exertions; SPL and Trap in extension exertions). The models predicted antagonist muscle (SPL and Trap in flexion exertions, SCM and Hyoid in extension exertions) inactivity, whereas only modest co-contractions were indicated by EMG. The average correlations (R^2) between model-predicted muscle tension and EMG-

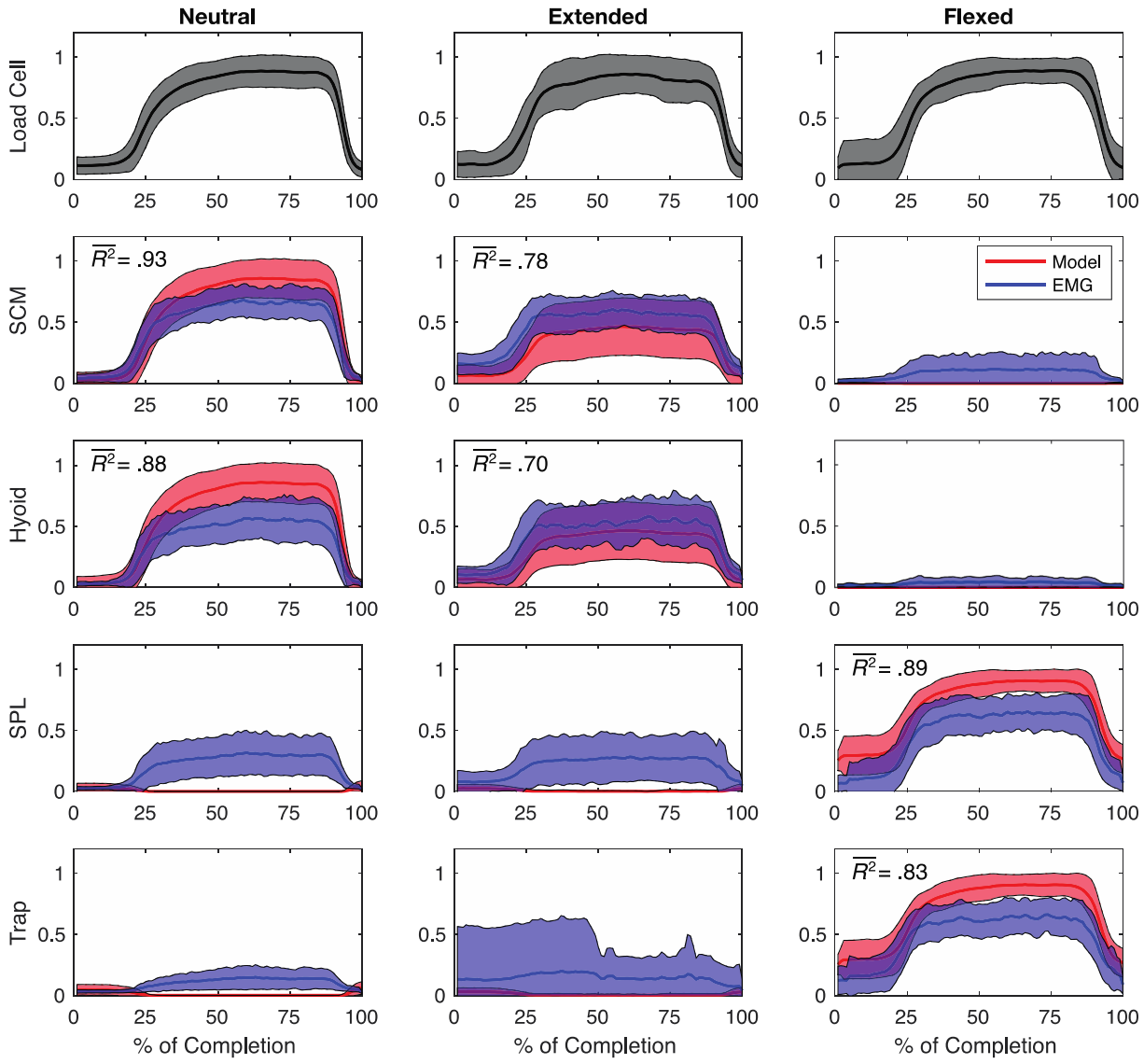

Fig. 3. Exertion forces recorded by load cell (top row) and model-predicted muscle tension vs. EMG profiles for four measured muscles (rows 2–4) scaled, normalized, and statistically summarized across all participants for three exertion postures (neutral, extended, and flexed). The solid lines represent the means and shaded areas represent the ± 1 standard deviation (SD).

measured muscle activation for the agonist muscles ranged from 0.70 to 0.93 (Fig. 3), and RMSEs ranged from 15.1 % to 25.7 % (Fig. 4).

3.2. Sex differences

Males, in general, have greater neck muscle moment arms, defined with respect to the center of the C6 vertebra near the base of the neck (Fig. 5 and Table 1). Among 10 neck muscles, significant sex differences were found in one flexor (Hyoids) and five extensor muscles (Deep, Longiss, SPL, SSCa, and LS). These significant differences were consistent in moment arms across the postures, which did vary but only by 6 % at most. No statistically significant differences between males and females in the variability of muscle moment arms was observed. It was also verified that participants' height or weight, did not have any correlation with their moment arm, for either sex.

Spinal compression forces at C6, predicted by the subject-specific models, were normalized by the corresponding exertion forces and compared between sexes across three postures (Fig. 6). In the neutral posture, spinal compression per unit of exertion force was moderately higher in males; in the flexed posture, spinal compression was substantially higher in females; in the extended posture, there was no statistically significant difference. Across all three postures, however, the variability of spinal compression was much greater in females than males, and the disparity was most pronounced in the extended posture.

4. Discussion

The present study was driven by an overarching goal to elucidate the biomechanical underpinning of sex differences in neck pain incidence and neck strength as a modifiable factor believed to play a role in injury prevention and treatment. An *in silico* approach was adopted wherein we constructed subject-specific biomechanical models incorporating individuals' unique musculoskeletal anatomies and used the models to digitally explore the hypothesized sex differences in neck structure and function and their pertinence to neck injury incidence. All model parameters and variables, obtained from imaging or biomechanical measurements, were subject-specific.

While more accurate anatomical representation of a model does not necessarily translate into more accurate biomechanical prediction, the accuracy of the presented subject-specific models appears to be

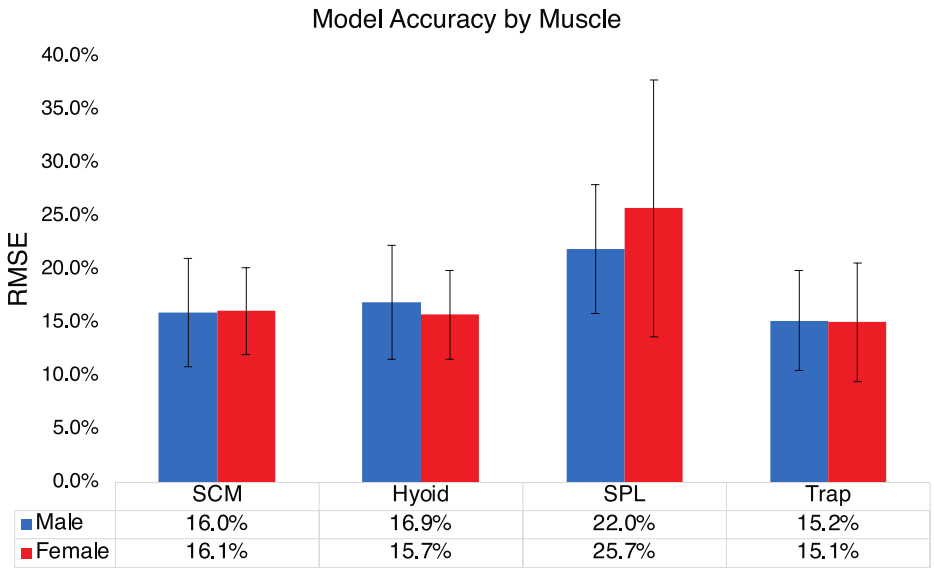

Fig. 4. Model accuracies assessed as RMSEs averaged across conditions comparing male and female and four muscle groups.

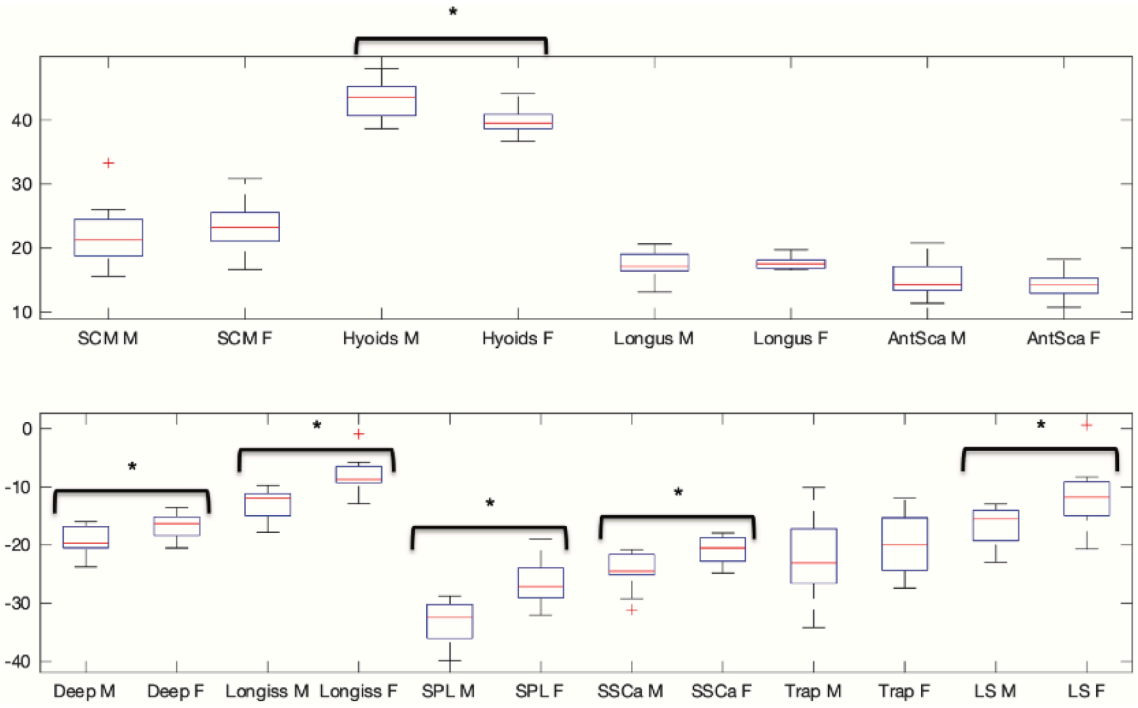

Fig. 5. Distributions of flexion (+) and extension (−) muscle moment arms (in mm) at C6 depicted as boxplots comparing males (M) and females (F). The red pluses indicate outliers and asterisks indicate statistically significant differences between sexes. The muscles included are sternocleidomastoid (SCM), infrahyoids (Hyoid), longus capitis + colli (Longus), anterior scalene (AntSca), semispinalis cervicis + multifidus (Deep), longissimus capitis and cervicis (Longiss), splenius capitis (SPL), semispinalis capitis (SSCa), upper trapezius (Trap), and levator scapula (LS). (For interpretation of the references to colour in this figure legend, the reader is referred to the web version of this article.)

comparable to or better than ones existing in the literature. The accuracy or validity of biomechanical models can be evaluated through a variety of qualitative and quantitative means. Prior neck modeling studies have evaluated accuracy by comparing models' moment generating capacity to *in vivo* human experimentation (Cazzola et al., 2017; Mortensen et al., 2018; Netto et al., 2008; Vasavada et al., 1998, 2001); however, this concept of model "accuracy" does not align with the general concept of validation in the broader field of biomechanical modeling, where comparing of EMG-measured muscle activity to model prediction is more common (Henninger et al., 2010; Hicks et al., 2015; Lund et al., 2012). Only one prior modeling study has quantified and reported mean absolute error (MAE) in muscle activity between EMG measurement and OpenSim model prediction (Trinler et al., 2018). It reported MAEs ranging from 13 – 69 % for some experimental conditions and used a 30 % MAE as a cut-off criterion for being "accurate." In this study, RMSE, a relatively higher magnitude metric than MAE due to an increased penalty for large deviations, was well below Trinler's criterion. Given this and the qualitative congruency seen between EMG and model-estimated muscle activation, the advanced subject-specific models generated using the proposed approach compare favorably in accuracy with existing

Table 1
Mean (SD) values of neck flexor (+) and extensor (−) muscle moment arms. Asterisks indicate significant sex differences.

Muscle Group:	SCM	Hyoids	Longus	AntSca	Deep
MALE	22.3 (4.8)	43.3 (2.9) *	17.6 (2.1)	15.1 (2.8)	−19.1 (2.5) *
FEMALE	23.4 (3.8)	39.7 (2.1) *	17.7 (1.0)	14.2 (2.0)	−16.8 (2.1) *
Muscle Group:	**Longiss**	**SPL**	**SSCa**	**Trap**	**LS**
MALE	−13.0 (2.5) *	−33.2 (3.6) *	−24.4 (3.3) *	−22.0 (6.9)	−16.5 (3.3) *
FEMALE	−8.1 (3.0) *	−26.6 (3.8) *	−20.8 (2.3) *	−20.0 (5.1)	−11.8 (5.4) *

neck and other biomechanical models.

The neck muscle moment arm data resulting from the current study constitute the most substantial and robust *in vivo* database to date. This is an addition to an earlier contribution of a neck muscle cross-sectional area database to the literature (Reddy et al., 2021). While muscle moment arm calculation methods are well established, actual data acquisition and analysis has been limited to small sample sizes, precluding any meaningful statistical exploration (Bonnefoy et al., 2007; Ingram et al., 2015). Vasavada et al. (1998) quantified muscle moment arms using a single model with generic anatomy and straight muscle paths, whereas Ackland et al. (2011) used five cadaveric head-neck complexes to study neck muscle moment arms based on the tendon excursion method. With a series of MR scans of two 50th percentile male subjects' neck regions in five different postures, Suderman and associates determined neck muscle moment arms and examined the effects of neck posture, muscle path representation, and moment arm calculation method using the MMP approach (Suderman et al., 2012; Suderman and Vasavada, 2017). The authors opted for MMP over the accepted and commonly used wrapping surface approach (Silvestros et al., 2021) citing lower deviations from anatomic centroid path and lower errors in trunk loading; though, MMP is not without its own disadvantages—primarily the assumption of muscle path adherence to a spline or polynomial curve even while under tension (Sherman et al., 2013). Their approach of using serial MRI and ours of using dynamic radiography along with a single MR scan both represent the state of the art in musculoskeletal geometry data acquisition. The two approaches can complement each other: the kinematics interpolated using the sequential MR scans can be improved using the "gold standard" skeletal motion data from dynamic radiography, whereas muscle deformation or path change extrapolated from skeletal motion can be verified and enhanced using MR imaging. Future endeavors combining both approaches could consummate the representation of moving and deforming neck muscles.

Findings from advanced subject-specific modeling shed new light on sex differences in neck biomechanics and injury propensity. We devised the metric of cervical spine disc compressive loading per unit exertion force as a surrogate measure to discern how individuals—males or females—differ in the transmission of external forces into internal stress. Significantly shorter moment arms for almost the entire extensor muscle group in females is the primary cause for substantially higher spine loading per unit exertion force experienced by females in extension with a flexed neck—the "dropped head" position most constantly assumed in work or leisure activities. This uncovers a plausible link connecting the biomechanical sex differences with the reported epidemiological sex difference in neck pain. Further, the greater variability of spinal compression in females may also be indicative of increased propensity for neck injury. Even in flexion exertions with a neutral or extended position where the mean spinal compression force was slightly lower in females, the dispersion for females was so much wider that a greater portion of the females than males would likely endure spinal loading exceeding the same injury threshold when meeting the same force requirement. It is noteworthy that there does not appear to be any sex difference in the variability of muscle moment arms, suggesting the sex disparity in spine loading variability arises from sources other than anatomical or morphological variability.

For the optimization-based muscle redundancy solution, this study formulated an objective function that minimized the sum of muscle stresses cubed, a function similar to what is used in most existing models and modeling tools including OpenSim. There is however one key difference: our formulation does not assume a universal maximum for muscle stress, referred to as *specific tension*, typically of fixed value of 35 N/cm^2 (Zajac, 1989). Rather, we allowed its variation across individuals and muscles, a choice that reflects the notion of personalization. Specific tension values for humans have been shown to vary in a wide range (Buchanan, 1995; Erskine et al., 2009; Fukunaga et al., 1996; Maganaris et al., 2001; O'Brien et al., 2010), although a more focused range for neck muscles is not available and merits further research. A well-recognized limitation of the optimization approach is that it precludes antagonist muscle activation, though some modest level of antagonist muscle co-contraction was observed through the EMG signals in the

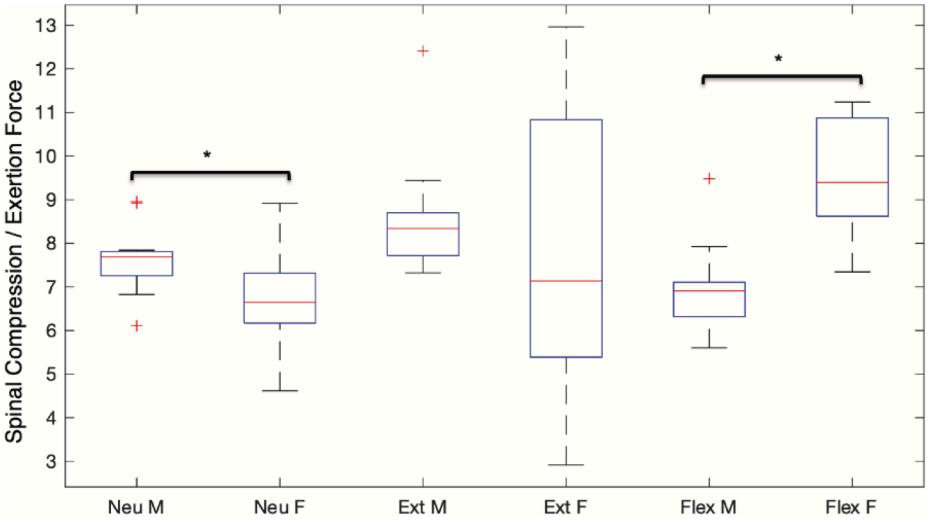

Fig. 6. Distributions of spinal compression per unit exertion force comparing males and females in three postures. Significant differences (asterisks) were noted in the neutral and flexed postures.

current study. While in this study the neck was modeled in isolation, cervical compressive forces may be affected by activation of other musculature in the body as would be commonplace in manual work environments and warrants future investigation. Additionally, a comparison between generic (scaled) and highly subject-specific models, utilizing an identical objective function, would better contextualize the impact of the new information gained from the novel modeling approach. Ultimately, the modeling framework constructed in the current study is intended to be a testbed for exploratory investigation into the variability of the neuromuscular components of neck biomechanics—a potential target for personalized clinical intervention.

CRediT authorship contribution statement

Curran Reddy: Writing – review & editing, Writing – original draft, Visualization, Validation, Investigation, Formal analysis, Conceptualization. **Yu Zhou:** Writing – review & editing, Writing – original draft, Investigation, Data curation, Conceptualization. **Wei Yin:** Writing – review & editing, Writing – original draft, Validation, Methodology, Investigation. **Xudong Zhang:** Writing – review & editing, Writing – original draft, Visualization, Validation, Supervision, Resources, Project administration, Methodology, Investigation, Funding acquisition, Formal analysis, Data curation.

Declaration of competing interest

The authors declare that they have no known competing financial interests or personal relationships that could have appeared to influence the work reported in this paper.

Acknowledgments

This work was supported by a research grant from the Centers for Disease Control and Prevention/National Institute for Occupational Safety and Health (Grant No. R01OH010587). Technical assistances provided by Dr. William Anderst of Department of Orthopaedic Surgery and Dr. Chan-Hong Moon of Department of Radiology at University of Pittsburgh Medical Center are acknowledged.

References

Ackland, D.C., Merritt, J.S., Pandy, M.G., 2011. Moment arms of the human neck muscles in flexion, bending and rotation. J. Biomech. 44, 475–486.
Barreto, T.W., Svec, J.H., 2019. Chronic neck pain: Nonpharmacologic treatment. Am. Fam. Physician 100, 180–182.
Bean, J.C., Chaffin, D.B., Schultz, A.B., 1988. Biomechanical model calculation of muscle contraction forces: A double linear programming method. J. Biomech. 21, 59–66.
Berglund, A., Bodin, L., Jensen, I., Wiklund, A., Alfredsson, L., 2006. The influence of prognostic factors on neck pain intensity, disability, anxiety and depression over a 2-year period in subjects with acute whiplash injury. Pain 125, 244–256.
Bolsterlee, B., Vardy, A.N., van der Helm, F.C., Veeger, H.D., 2015. The effect of scaling physiological cross-sectional area on musculoskeletal model predictions. J. Biomech. 48, 1760–1768.
Bonnefoy, A., Doriot, N., Senk, M., Dohin, B., Pradon, D., Cheze, L., 2007. A non-invasive protocol to determine the personalized moment arms of knee and ankle muscles. J. Biomech. 40, 1776–1785.
Buchanan, T., 1995. Evidence that maximum muscle stress is not a constant: Differences in specific tension in elbow flexors and extensors. Med. Eng. Phys. 17, 529–536.
Cazzola, D., Holsgrove, T.P., Preatoni, E., Gill, H.S., Trewartha, G., 2017. Cervical spine injuries: A whole-body musculoskeletal model for the analysis of spinal loading. PLoS One 12, e0169329.
Chowdhury, S.K., Zhou, Y., Wan, B., Reddy, C., Zhang, X., 2021. Neck strength and endurance and associated personal and work-related factors. Hum. Factors.
Clancy, E.A., Morin, E.L., Merletti, R., 2002. Sampling, noise-reduction and amplitude estimation issues in surface electromyography. J Electromyogr Kinesiol 12, 1–16.
Connor, T.A., Colgan, N., Stewart, M., Ní Annaidh, A., Gilchrist, M.D., 2020. Inertial properties of a living population for the development of biofidelic headforms. Proceedings of the Institution of Mechanical Engineers, Part P: Journal of Sports Engineering and Technology, 1754337120921646.
Côté, J.N., 2012. A critical review on physical factors and functional characteristics that may explain a sex/gender difference in work-related neck/shoulder disorders. Ergonomics 55, 173–182.
Côté, P., Cassidy, J.D., Carroll, L.J., Kristman, V., 2004. The annual incidence and course of neck pain in the general population: A population-based cohort study. Pain 112, 267–273.
Dieleman, J.L., Baral, R., Birger, M., Bui, A.L., Bulchis, A., Chapin, A., Hamavid, H., Horst, C., Johnson, E.K., Joseph, J., 2016. Us spending on personal health care and public health, 1996–2013. JAMA 316, 2627–2646.
Dolinis, J., 1997. Risk factors for 'whiplash' in drivers: A cohort study of rear-end traffic crashes. Injury 28, 173–179.
Eiter, T., Mannila, H., 1994. Computing discrete fréchet distance, Technical report CD-TR 94/64. Technische Universitat Wien.
Erdemir, A., McLean, S., Herzog, W., van den Bogert, A.J., 2007. Model-based estimation of muscle forces exerted during movements. Clin. Biomech. 22, 131–154.
Erskine, R.M., Jones, D.A., Maganaris, C.N., Degens, H., 2009. In vivo specific tension of the human quadriceps femoris muscle. Eur. J. Appl. Physiol. 106, 827.
Evans, G., 2014. Identifying and treating the causes of neck pain. Medical Clinics 98, 645–661.
Fukunaga, T., Roy, R., Shellock, F., Hodgson, J., Edgerton, V., 1996. Specific tension of human plantar flexors and dorsiflexors. J. Appl. Physiol. 80, 158–165.
Hendriks, E.J., Scholten-Peeters, G.G., van der Windt, D.A., Neeleman-van der Steen, C. W., Oostendorp, R.A., Verhagen, A.P., 2005. Prognostic factors for poor recovery in acute whiplash patients. Pain 114, 408–416.
Henninger, H.B., Reese, S.P., Anderson, A.E., Weiss, J.A., 2010. Validation of computational models in biomechanics. Proc. Inst. Mech. Eng. [H] 224, 801–812.
Hicks, J.L., Uchida, T.K., Seth, A., Rajagopal, A., Delp, S.L., 2015. Is my model good enough? Best practices for verification and validation of musculoskeletal models and simulations of movement. J. Biomech. Eng. 137.
Hoy, D., March, L., Woolf, A., Blyth, F., Brooks, P., Smith, E., Vos, T., Barendregt, J., Blore, J., Murray, C., 2014. The global burden of neck pain: Estimates from the global burden of disease 2010 study. Ann. Rheum. Dis. 73, 1309–1315.
Hughes, R.E., Chaffin, D.B., Lavender, S.A., Andersson, G.B., 1994. Evaluation of muscle force prediction models of the lumbar trunk using surface electromyography. J. Orthop. Res. 12, 689–698.
Hurwitz, E.L., Randhawa, K., Yu, H., Côté, P., Haldeman, S., 2018. The global spine care initiative: A summary of the global burden of low back and neck pain studies. Eur. Spine J. 27, 796–801.
Ingram, D., Engelhardt, C., Farron, A., Terrier, A., Müllhaupt, P., 2015. Muscle moment-arms: A key element in muscle-force estimation. Comput. Methods Biomech. Biomed. Eng. 18, 506–513.
Kamibayashi, L.K., Richmond, F.J., 1998. Morphometry of human neck muscles. Spine 23, 1314–1323.
Lund, M.E., de Zee, M., Andersen, M.S., Rasmussen, J., 2012. On validation of multibody musculoskeletal models. Proc. Inst. Mech. Eng. [H] 226, 82–94.
Maganaris, C.N., Baltzopoulos, V., Ball, D., Sargeant, A.J., 2001. In vivo specific tension of human skeletal muscle. J. Appl. Physiol. 90, 865–872.
McGill, S.M., Norman, R.W., 1987. Effects of an anatomically detailed erector spinae model on l4/l5 disc compression and shear. J. Biomech. 20, 591–600.
Millard, M., Uchida, T., Seth, A., Delp, S.L., 2013. Flexing computational muscle: Modeling and simulation of musculotendon dynamics. J. Biomech. Eng. 135.
Mortensen, J.D., Vasavada, A.N., Merryweather, A.S., 2018. The inclusion of hyoid muscles improve moment generating capacity and dynamic simulations in musculoskeletal models of the head and neck. PLoS One 13, e0199912.
Murray, C.J., Abraham, J., Ali, M.K., Alvarado, M., Atkinson, C., Baddour, L.M., Bartels, D.H., Benjamin, E.J., Bhalla, K., Birbeck, G., 2013. The state of us health, 1990–2010: Burden of diseases, injuries, and risk factors. JAMA 310, 591–606.
Netto, K.J., Burnett, A.F., Green, J.P., Rodrigues, J.P., 2008. Validation of an EMG-driven, graphically based isometric musculoskeletal model of the cervical spine. J. Biomech. Eng. 130.
O'Brien, T.D., Reeves, N.D., Baltzopoulos, V., Jones, D.A., Maganaris, C.N., 2010. In vivo measurements of muscle specific tension in adults and children. Exp. Physiol. 95, 202–210.
Reddy, C., Zhou, Y., Wan, B., Zhang, X., 2021. Sex and posture dependence of neck muscle size-strength relationships. J. Biomech., 110660
Saraswat, P., Andersen, M.S., MacWilliams, B.A., 2010. A musculoskeletal foot model for clinical gait analysis. J. Biomech. 43, 1645–1652.
Seth, A., Sherman, M., Reinbolt, J.A., Delp, S.L., 2011. Opensim: A musculoskeletal modeling and simulation framework for in silico investigations and exchange. Procedia Lutam 2, 212–232.
Seth, A., Hicks, J.L., Uchida, T.K., Habib, A., Dembia, C.L., Dunne, J.J., Ong, C.F., DeMers, M.S., Rajagopal, A., Millard, M., 2018. Opensim: Simulating musculoskeletal dynamics and neuromuscular control to study human and animal movement. PLoS Comput. Biol. 14.
Sherman, M.A., Seth, A., Delp, S.L., 2013. What is a moment arm? Calculating muscle effectiveness in biomechanical models using generalized coordinates. In: International design engineering technical conferences and computers and information in engineering conference, Vol. 55973. American Society of Mechanical Engineers, V07BT10A052.
Silvestros, P., Pizzolato, C., Lloyd, D.G., Preatoni, E., Gill, H.S., Cazzola, D., 2021. Electromyography-assisted neuromusculoskeletal models can estimate physiological muscle activations and joint moments across the neck before impacts. J. Biomech. Eng. 144.
Suderman, B.L., Krishnamoorthy, B., Vasavada, A.N., 2012. Neck muscle paths and moment arms are significantly affected by wrapping surface parameters. Comput. Methods Biomech. Biomed. Eng. 15, 735–744.
Suderman, B.L., Vasavada, A.N., 2017. Neck muscle moment arms obtained in-vivo from mri: Effect of curved and straight modeled paths. Ann. Biomed. Eng. 45, 2009–2024.

Trinler, U., Leboeuf, F., Hollands, K., Jones, R., Baker, R., 2018. Estimation of muscle activation during different walking speeds with two mathematical approaches compared to surface EMG. Gait Posture 64, 266–273.
Vasavada, A.N., Li, S., Delp, S.L., 1998. Influence of muscle morphometry and moment arms on the moment-generating capacity of human neck muscles. Spine 23, 412–422.
Vasavada, A.N., Li, S., Delp, S.L., 2001. Three-dimensional isometric strength of neck muscles in humans. Spine 26, 1904–1909.
Vos, T., Flaxman, A.D., Naghavi, M., Lozano, R., Michaud, C., Ezzati, M., Shibuya, K., Salomon, J.A., Abdalla, S., Aboyans, V., 2012. Years lived with disability (YLDS) for 1160 sequelae of 289 diseases and injuries 1990–2010: A systematic analysis for the global burden of disease study 2010. Lancet 380, 2163–2196.
Ylinen, J., Takala, E.-P., Nykänen, M., Häkkinen, A., Mälkiä, E., Pohjolainen, T., Karppi, S.-L., Kautiainen, H., Airaksinen, O., 2003. Active neck muscle training in the treatment of chronic neck pain in women: A randomized controlled trial. JAMA 289, 2509–2516.
Yoganandan, N., Pintar, F.A., Zhang, J., Baisden, J.L., 2009. Physical properties of the human head: Mass, center of gravity and moment of inertia. J. Biomech. 42, 1177–1192.
Zajac, F.E., 1989. Muscle and tendon: Properties, models, scaling, and application to biomechanics and motor control. Crit. Rev. Biomed. Eng. 17, 359–411.
Zheng, L., Siegmund, G., Ozyigit, G., Vasavada, A., 2013. Sex-specific prediction of neck muscle volumes. J. Biomech. 46, 899–904.
Zhou, Y., Reddy, C., Wan, B., Chowdhury, S., Zhang, X., 2019. Piecewise multi-modal spine registration to build personalized neck musculoskeletal models. International/American Society of Biomechanics Calgary, Canada.
Zhou, Y., Chowdhury, S., Reddy, C., Wan, B., Byrne, R., Yin, W., Zhang, X., 2020a. A state-of-the-art integrative approach to studying neck biomechanics in vivo. Sci. China Technol. Sci. 1–12.
Zhou, Y., Reddy, C., Wan, B., Yin, W., Zhang, X., 2020b. Pose-matching MRI-CT co-registration via dynamic x-ray for creating subject-specific neck musculoskeletal models. American Society of Biomechanics, Atlanta, GA.